

## Accepted Manuscript

Synthesis, structural characterization and Hirshfeld analysis studies of three novel co-crystals of trans- 4-[(2-amino-3, 5-dibromobenzyl) amino] cyclohexanol with hydroxyl benzoic acids

Yu-heng Ma, Ming Lou, Qing-yang Sun, Shu-wang Ge, Bai-wang Sun

PII: S0022-2860(14)01132-6

DOI: <http://dx.doi.org/10.1016/j.molstruc.2014.11.026>

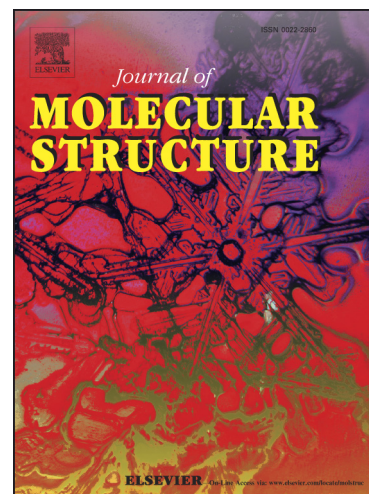
Reference: MOLSTR 21104

To appear in: *Journal of Molecular Structure*

Received Date: 18 June 2014

Revised Date: 10 November 2014

Accepted Date: 10 November 2014



Please cite this article as: Y-h. Ma, M. Lou, Q-y. Sun, S-w. Ge, B-w. Sun, Synthesis, structural characterization and Hirshfeld analysis studies of three novel co-crystals of trans- 4-[(2-amino-3, 5-dibromobenzyl) amino] cyclohexanol with hydroxyl benzoic acids, *Journal of Molecular Structure* (2014), doi: <http://dx.doi.org/10.1016/j.molstruc.2014.11.026>

This is a PDF file of an unedited manuscript that has been accepted for publication. As a service to our customers we are providing this early version of the manuscript. The manuscript will undergo copyediting, typesetting, and review of the resulting proof before it is published in its final form. Please note that during the production process errors may be discovered which could affect the content, and all legal disclaimers that apply to the journal pertain.

**Synthesis, structural characterization and Hirshfeld analysis studies of three novel co-crystals of trans- 4-[(2-amino-3, 5-dibromobenzyl) amino] cyclohexanol with hydroxyl benzoic acids**

Yu-heng Ma<sup>[a]</sup>, Ming Lou<sup>[a]</sup>, Qing-yang Sun<sup>[b]</sup>, Shu-wang Ge<sup>[a]</sup>, Bai-wang Sun<sup>[a]</sup> \*

[a] School of Chemistry and Chemical Engineering, Southeast University, Nanjing 210096, P. R. China

[b] Screening Test Department, Hangzhou 117 hospital, Hangzhou 310000, P. R. China

Telephone number: 86-25-52090614

Fax number: 86-25-52090614

Email: chmsunbw@seu.edu.cn

# Synthesis, structural characterization and Hirshfeld analysis studies of three novel co-crystals of trans- 4-[(2-amino-3, 5-dibromobenzyl) amino] cyclohexanol with hydroxyl benzoic acids

Yu-heng Ma, Ming Lou, Qing-yang Sun, Shu-wang Ge, Bai-wang Sun\*

*School of Chemistry and Chemical Engineering, Southeast University, Nanjing 210096, P. R. China*

Telephone: 86-25-52090614, Fax: 86-25-52090614, E-mail: chmsunbw@seu.edu.cn

## Abstract:

Combination of Active Pharmaceutical Ingredients, trans-4-[(2-amino-3, 5-dibromobenzyl) amino] cyclohexanol (AMB) and some organic acids, e.g., p-hydroxybenzoic acid (PHBA), m-hydroxybenzoic acid (MHBA), and 3, 4-dihydroxy benzoic acid (DHBA), yield three novel co-crystals characterized by X-ray single-crystal, Fluorescence spectroscopy and thermal analysis (DSC and TGA), which included co-crystal **1** with 2: 2: 1 stoichiometry of AMB, PHBA and H<sub>2</sub>O, co-crystal **2** with 1: 1 stoichiometry of AMB and MHBA, and co-crystal **3** with 1: 1: 1 stoichiometry of AMB, DHBA and CH<sub>3</sub>OH. Constituents of the co-crystalline phase were also investigated in terms of Hirshfeld surfaces. In the crystal lattice, a three-dimensional hydrogen-bonded network is observed, including formation of a two-dimensional molecular scaffolding motif. Hirshfeld surfaces and fingerprint plots of three co-crystals show that structures are stabilized by H...H, N-H...O, H...Br and C...H intermolecular interactions. Besides, the studies of the solubility showed that this co-crystal strategy could promote the solubility of AMB and follow the order: co-crystal **1** < co-crystal **2** < co-crystal **3**.

**Keywords:** Co-crystal; Ambroxol; Hydroxybenzoic acid; Hirshfeld surface; Fluorescence spectroscopy; Hydrogen-bond

## 1. Introduction

The term co-crystal was first coined in the perspective of complexes between nucleic bases and later it was subsequently popularized by Etter<sup>[1-6]</sup>. Although the definition of co-crystal is often a topic of debate, co-crystal has gained a lot of recent attention owing to its amenability to design and tailor physiochemical properties like solubility, dissolution, stability and bioavailability, which play a major role in the development of an active pharmaceutical ingredient (API) into a drug candidate<sup>[7-9]</sup>. Some of the co-crystals could display unique properties differing from the individual co-crystal formers.<sup>[10-15]</sup>

Ambroxol is a secretolytic agent which was used in the treatment of respiratory diseases associating with viscid or excessive mucus. The substance is a mucoactive drug with several properties including secretolytic and secretomotoric actions that restore the physiological clearance mechanisms of the respiratory tract, which plays an important role in the body's natural defense mechanisms. It stimulates synthesis and release of surfactant by type II pneumocytes<sup>[16-17]</sup>. As a continuation of our recent study on the Ambroxol salts and different aromatic carboxylic acids, we report on the synthesis, crystal structures and analysis of intermolecular interactions, especially those involving crystal packing of three novel co-crystals (**Scheme 1**). These co-crystals were characterized by single-crystal X-ray diffraction, thermal analysis (DSC and TGA) and Hirshfeld surfaces analysis, details are as follows.

## 2. Theoretical calculation

Molecular Hirshfeld surfaces are prepared by using the CrystalExplorer<sup>[18-20]</sup> computer program. It is a space partitioning construct that summarizes the crystal packing into a color-schemed single 3D surface and the surface can be reduced to a 2D fingerprint plot, which summarizes the complex information on the intermolecular interactions presenting in molecular crystals. The principles of Hirshfeld surfaces were reported in the literature<sup>[21-24]</sup>. In this work, we studied the intermolecular interactions in co-crystals **1-3** qualitatively and quantitatively.

## 3. Experimental section

### 3.1 Preparation of co-crystals 1-3

The preparation of co-crystals **1-3** were shown in **Scheme 2**. Ambroxol hydrochloride was neutralized by NaOH (1mol/ L) in water and the mixture was poured into CH<sub>2</sub>Cl<sub>2</sub>, which was then extracted, dried with anhydrous sodium sulfate, and evaporated under reduced pressure to give Ambroxol as colourless oil. The co-crystals **1-3** were prepared by mixing Ambroxol with the corresponding acids in suitable solvent. A general experimental procedure for co-crystal **1** is as follows: AMB (1mmol, 378.1 mg) and PHBA (1mmol, 138.2mg) were dissolved in 20 ml methanol / water (1:1). Then the solution was stirred for 1 h, filtered and left for slow evaporation under ambient conditions to yield co-crystal.

### 3.2 Physical measurements

The differential scanning calorimetry (DSC) and thermogravimetric analysis (TGA) were performed using a Mettler-Toledo TGA/DSC STAR<sup>c</sup> system at a heating rate of 10 Kmin<sup>-1</sup> under an atmosphere of dry N<sub>2</sub> flowing at 20 cm<sup>3</sup> min<sup>-1</sup> over a range from 40°C to 400°C. Samples were placed in open aluminum oxide crucibles annealed at 1100°C. The TGA/DSC datas were analyzed by using STAR<sup>c</sup> software.

### 3.3 X-ray crystallographic study

The single crystal X-ray diffraction datas of co-crystals **1-3** were collected at 293K with graphite monochromated Mo-K $\alpha$  radiation ( $\lambda=0.071073\text{nm}$ ), and a Rigaku SCXmini diffractometer with the  $\omega$ -scan technique was used. The lattice parameters were integrated using vector analysis and refined from the diffraction matrix, and the absorption correction was carried out by using Bruker SADABS program with the multi-scan method. A summary of crystallographic data, data collection, and refinement parameters for co-crystals **1-3** are summarized in **Table 1**. Their structures were solved by full-matrix least-squares methods on all F<sup>2</sup> data, and the SHELXS-97 and SHELXL-97 programs<sup>[25]</sup> were used for structure solution and structure refinement respectively. Reliability factors were defined as  $R_1 = \sum_w(|F_0| - |F_c|) / \sum |F_0|$  and the function minimized was  $R_w = [\sum_w(F_0^2 - F_c^2)^2 / w(F_0^4)]^{1/2}$ , where in the least-squares calculation the unit weight was used. All non-hydrogen atoms were refined anisotropically,

and hydrogen atoms were inserted at their calculated positions and fixed at their positions <sup>[26-27]</sup>. The molecular graphics were prepared by using the mercury program <sup>[28]</sup>. CCDC reference numbers 938703, 938704 and 938702 contain the supplementary crystallographic data in CIF format for co-crystals **1-3** reported in this paper. These data can be obtained free of charge from The Cambridge Crystallographic Data Centre via [www.ccdc.cam.ac.uk/data\\_request/cif](http://www.ccdc.cam.ac.uk/data_request/cif).

### 3.4 Hirshfeld surface calculations

Molecular Hirshfeld surfaces calculations were performed by using the CrystalExplorer program. When the CIF files of co-crystals **1-3** are read into the CrystalExplorer program, all bond lengths to hydrogen were automatically modified to typical standard neutron values (C–H= 1.083 Å and N–H= 1.009 Å). In this study, all the Hirshfeld surfaces were generated using a standard (high) surface resolution. The 3-D  $d_{norm}$  surfaces were mapped by using a fixed color scale of 0.76 (red) to 2.4 Å (blue), shape index mapped in the color range of 0.7-2.5, and curvedness in the range of 0.72-2.4. The 2-D fingerprint plots were displayed by using the standard 0.6–2.6 Å view with the  $d_e$  and  $d_i$  distance scales displayed on the graph axes.

### 3.5 Solubility studies

A Waters Alliance 2695 HPLC system was used to analyze co-crystals **1-3**, together with a 996 Photodiode Array (PDA) detector. A Kromasil C18 analytical column (250 mm × 2.1 mm, 5 μm particle size) was used as a separation column. For ambroxol analysis, the UV detector was set at a wavelength of 210 nm. A mixture of Diammonium Phosphate 0.05 M and methanol (55:45) was used as the mobile phase. The column temperature was maintained at 45 °C during analysis. Pretreatment and concentration columns were operated at ambient temperature. Pumps 1 and 2 were used to deliver mobile phase 1 at a flow rate of 0.55 ml /min and mobile phase 2 at a flow rate of 0.45 ml/min, respectively. The entire solution was filtered using a 0.45 μm membrane filter (Millipore Corp., Bedford) and degassed before running the HPLC analysis. The system was run at 1 ml min<sup>-1</sup> flow rate and the running time was 30 min. The injection volume was 10 μl.

## 4. Results and Discussion

### 4.1 Crystal structures

Co-crystal **1** crystallizes as pink cuboid-shaped crystals. The structural determination shows it forms a 2: 2: 1 (AMB: PHBA: H<sub>2</sub>O) co-crystal in the monoclinic P2/c space group with Z = 2, the asymmetric unit consisting of one entire H<sub>2</sub>O molecule, two entire AMB molecules and two PHBA molecules. The H<sub>2</sub>O molecule formed a tetrahedral structure with two AMB molecules and two PHBA molecules through O–H···O ( distance of 2.698 Å and 2.660 Å, angle of 174° and 132°) hydrogen bond interactions (**Figure 1a**) and it also involved in the formation of a pentameric unit by R<sub>5</sub><sup>5</sup>(22) supramolecular heterosynthon through O–H···O (distance of 2.639 Å, 2.734 Å, 2.711 Å and 2.660 Å) hydrogen bond interactions.

Then two AMB molecules and two PHBA molecules formed a tetrameric unit by R<sub>4</sub><sup>4</sup>(8) supramolecular heterosynthon through O–H···N (distance of 2.778 Å and 2.755 Å) and N–H···O (distance of 2.770 Å and 2.767 Å) hydrogen bond interactions (**Figure 1b**). For each PHBA, it also formed dimeric unit with a AMB molecule by R<sub>2</sub><sup>2</sup>(8) supramolecular heterosynthon through N–H···O (distance of 2.942 Å and angle of 121°) and O–H···N (distance of 2.755 Å and angle of 165°) hydrogen bond interactions (**Figure 1c**).

Further analysis of co-crystal **1** in three-dimension reveals stacked layer structure. The arrangement of molecules in a typical layer is shown in **Figure 1d**. Within the layer viewed from b-axis, the AMB molecules displayed as an infinite 1D chain. Then H<sub>2</sub>O and PHBA molecules play very important roles in the formation of network structure, which was held by different types of C–H···π interaction with the distance of 3.478, 3.576, 3.761 and 3.551 Å (**Table 2**). When viewed from the a-axis, the molecules are held by a series of hydrogen bonds. When viewed from the c- axis, the layer stacked crossly with each other along the a-axis, and an obvious π···π intermolecular interactions were observed with plane separation of 3.776 Å (**Figure 1e**). Geometrical parameters for hydrogen bonds, C–H···π and π···π and

Br $\cdots$ X (-H, -C, or -Br) interactions in co-crystals **1-3** were all summarized in **Table 2**.

Co-crystal **2** crystallizes as colorless cuboid-shaped crystals. The structural determination shows it forms a 1: 1 (AMB: MHBA) co-crystal in the monoclinic  $p21/n$  space group with  $Z = 4$ , the asymmetric unit consisting of three entire AMB molecules and three entire MHBA molecules. Two AMB molecules and two entire MHBA molecules involved in the formation of a tetrameric unit by  $R_4^4(20)$  supramolecular heterosynthon through O–H $\cdots$ O (distance of 2.621 Å) and N–H $\cdots$ O (distance of 2.819 Å and 2.733 Å) hydrogen bonds (**Figure 2a**), and the same tetrameric units then connected with six other units into a zigzag motif (**Figure 2c**). Obviously, co-crystal **2** also has a stacked layer structure. The arrangement of molecules in a typical layer is shown in **Figure 2c** and the width of each layer is 13.883 Å. The angle of the benzene rings in two MHBA molecules is 33.88° and the benzene rings of two AMB molecules are nearly perpendicular (angle of 84.06°). It was interesting that no C–H $\cdots$  $\pi$  and  $\pi\cdots\pi$  interactions were detected in its crystal structure; a Br $\cdots$ Br interaction<sup>[29]</sup> aroused our attention in **Figure 2b** which is at a van der Waals distance of  $-0.11$  Å (distance of 3.585 Å). This interaction plays an important role in stabilizing the structure of co-crystal **2**.

Co-crystal **3** is brown cuboid-shaped crystal. The structure determination shows it forms a 1:1:1(AMB: DHBA: CH<sub>3</sub>OH) co-crystal in the monoclinic  $Cc$  space group with  $Z = 2$ , the asymmetric unit consisting of two entire AMB molecules, two entire DHBA molecules and two CH<sub>3</sub>OH molecules. Two AMB molecules and two entire DHBA molecules involved in the formation of a tetrameric unit by  $R_4^4(8)$  supramolecular heterosynthon through O–H $\cdots$ O (distance of 2.686 Å and 2.677 Å) and N–H $\cdots$ O (distance of 2.761 Å and 2.861) hydrogen bond interactions (**Figure 3a**). Then one AMB molecule and one DHBA molecule also involved in the formation of a dimeric unit by  $R_2^2(10)$  supramolecular heterosynthon through N–H $\cdots$ O (distance of 2.761 Å and 2.914 Å) hydrogen bond interactions (**Figure 3b**). The CH<sub>3</sub>OH molecule as a bridge connected two DHBA molecules through O–H $\cdots$ O (distance of 2.630 Å and 2.628 Å)

hydrogen bond interactions (**Figure 3c**). In this crystal lattice, a two-dimensional network is observed (**Figure 3d and 3e**) and a C-H... $\pi$  interactions was detected with the distance of 3.588 Å. Analyzing the crystal structure among the co-crystals **1-3**, it is obvious that co-crystals **1-2** have a stacked layer structure, but it does not exist in co-crystal **3**.

#### 4.2 Hirshfeld surfaces analysis

Hirshfeld surface and fingerprint plot analysis could offer rapid reckonable understanding into the intermolecular interactions in complex molecular solids as well as crystal structures by color-coding short or long contacts, which acts as an easier and considerably faster graphical tool which is based on 3D Hirshfeld surfaces and 2D fingerprint plots, and gives a quantitative summary of the nature and type of intermolecular contacts experienced by the molecules in the crystal. In this section, we investigated the molecular Hirshfeld surface of AMB in the co-crystals **1-3**, to elucidate the features of different supramolecular synthons.

The 3D Hirshfeld surfaces and 2D fingerprint plots of AMB in co-crystals **1-3** are shown in **Figure 4**. They clearly show the influences of different co-formers on the intermolecular interactions of the AMB molecule. The large and deep red spots on the 3D Hirshfeld surfaces indicate the close-contact interactions, which are mainly responsible for the significant hydrogen bonding contacts. The small red spots on the surfaces represent the C-H... $\pi$  and H...Br interactions, while the red color points in the 2D fingerprint plots are indicative of short contacts of H...H, H...N, and H...O interactions.

For co-crystal **1** (**Figure 4a**), H...H interactions, which are reflected in the middle of scattered points in the 2D fingerprint plots, have the most significant contribution (29.1%) to the total Hirshfeld surfaces. The N-H...O hydrogen bonding intermolecular interactions appear as a fork in the 2D fingerprint plots, which have 24.5% contribution to the total Hirshfeld surfaces. While O-H...N hydrogen bonding interactions appear as a single, sharp spike in the 2D fingerprint plots and only comprises 5.2% of the total Hirshfeld surfaces. The C-H... $\pi$  interactions also have a relatively significant contribution to the total Hirshfeld surfaces of co-crystal **1**, comprised of 13.5%, which was reflected in the lower right of the 2D fingerprint

plot. Apart from those above, the presence lone-pair...lone-pair (O–N), C–Br... $\pi$ , H...Br, Br...Br and Br...O interactions are observed, which are summarized in **Table 3**.

The Hirshfeld surface analysis for AMB in co-crystal **2** was all illustrated in **Figure 4b**. Unlike co-crystal **1** and co-crystal **3**, the H...Br interactions have the second strong significant contribution to the total Hirshfeld surfaces (21.8%) rather than H...O interactions (18.5%). The H...H interactions also contribute most to the total Hirshfeld surfaces (35.7%), which is as same as the H...H interactions in co-crystal **1** and co-crystal **3**. The C–H... $\pi$ , N...H and C...Br interactions are in the corner of the 2D fingerprint plots, and comprise 17.8%, 2.0% and 1.5% to the total Hirshfeld surfaces.

The Hirshfeld surface analysis for AMB in co-crystal **3** (**Figure 4c**) was similar to co-crystal **1**. The H...H interactions have the most significant contribution to the total Hirshfeld surfaces, which comprise 38.6%. The O...H–N hydrogen bonding interaction was a little larger than that in co-crystal **2**, comprised of 20.8%. The H...Br interactions have the third significant contribution to the total Hirshfeld surfaces (19.8%), which is a little larger than that in co-crystal **1**. The C–H... $\pi$ , N...H, C...Br, O...Br interactions are in the corner of the 2D fingerprint plots, and comprise 16%, 1.2%, 0.9% and 1.6 to the total Hirshfeld surfaces. The weaker Br...Br interactions of co-crystal are absent possibly because of lacking of stacked layer structure in co-crystal **3**. As inferred from the geometrical analysis, the most interesting thing is that the H...H interactions all have the most significant contribution to the total Hirshfeld surfaces, especially for co-crystal **3** (38.6%), which has more hydroxyl group and form more hydrogen bonds than co-crystal **1** and co-crystal **2**, suggesting that the co-crystal **3** is the most stable structure in three co-crystals.

#### **4.3 Differential scanning calorimetry (DSC) and thermogravimetric analysis (TGA) of co-crystals 1-3**

The DSC and TGA curves of three co-crystals in nitrogen atmosphere at a heating rate of 10 Kmin<sup>-1</sup> with a temperature range of 40~400°C are shown in **Figure 5**. We can see from DSC curves that co-crystal **1**(AMB-PHBA-1/2H<sub>2</sub>O) melts at approximately 155.3°C with a melting enthalpy of 96.05Jg<sup>-1</sup>.

And then TGA curves show a weight loss about 1.8%. It could be due to decomposition of the guest H<sub>2</sub>O molecules, which is included in the crystal lattice. From 183°C to 240°C, the TGA shows a significant mass loss about 27% and it could be due to the guest PHBA molecules. Then the thermal decomposition process of AMB molecule started from 280°C, and the exothermic peak is found at 300.5°C. By 320°C, the decomposition is also nearly complete, and the TGA shows mass loss about 30%. And it could be AMB molecules degradation accompanying with bromine evolution. For co-crystal **2** (AMB-MHBA), the thermal behavior is very different from that of co-crystal **1**. It undergoes two steps of mass loss on TGA. The first step is a mass loss of about 27% at approximately 182.5°C with a melting enthalpy of 109.9 Jg<sup>-1</sup>, which is attributed to the decomposition of guest MHBA molecules. The second step is a mass loss of 31% at approximately 295.1 °C, which is also due to the bromine evolution. For co-crystal **3** (AMB-DHBA-CH<sub>3</sub>OH), DSC curves corresponding to TGA curves have two endothermic peaks and one exothermic peak. When co-crystal **3** began to lose weight, DSC curves have an obvious endothermic peak at 135.9°C with a melting enthalpy of 134.2 Jg<sup>-1</sup>. And the mass loss is about 5.5%. It could be due to the guest CH<sub>3</sub>OH molecules, which is also included in the crystal lattice. The second endothermic process is not very obvious and the endothermic peak is found at 198.5°C. The corresponding mass loss is about 27.5%, which is could be the guest DHBA molecules. The last exothermic process is due to the bromine evolution and the exothermic peak is found at 298.1°C.

#### 4.4 Fluorescence spectroscopy

Fluorescence emission spectra were exploited to investigate the optical-properties of co-crystals **1-3**, and the fluorescent properties have been investigated in the solid state at room temperature. In **Figure 6a**, we found co-crystal **1** has the largest fluorescence intensity among three co-crystals. Excited at 350 nm,

crystal **1** exhibits a broad emission band around 370-480 nm with one peaks at 425 nm. However, excited at 370 nm, the spectrum of co-crystals **1-3** all exhibit a band around 400-530 nm (the peak at 424 nm for co-crystal **1**, the peak at 435 nm for co-crystal **2** and the peak at 452 nm for co-crystal **3**) in **Figure 6b**. Compared with the fluorescence of Ambroxol, the broad emission bands with a red shift of about 10 nm of co-crystal **1** and the broad emission bands with blue shift of about 18 nm for co-crystal **3** should be caused by hydrogen bonding between guest molecules and host molecule while co-crystal **2** shows no apparent movement. We also found the emission wavelength of three co-crystals follow the order: co-crystal **1** < co-crystal **2** < co-crystal **3** which is consistent with H...H interactions of Hirshfeld surfaces analysis: co-crystal **1** (29.1%) < co-crystal **2** (35.7%) < co-crystal **3** (38.6%).

Although we cannot give further explanations for the relationship between the solid-state emission properties and hirshfeld surfaces analysis, guest molecules and crystal structure, the strategy provides a facile way to design and develop new co-crystals with interesting solid fluorescent properties.

#### 4.4 Solubility studies

Solubility is an important parameter for the estimation of bioavailability of pharmaceutical. In this paper, High Performance Liquid Chromatography (HPLC) was employed to investigate the solubility of co-crystals **1-3** which has major advantages in terms of sensitivity and specificity. Prior to solubility measurements, Stock solutions of AMB (1mg/ml) were prepared in methanol and were serially diluted with mobile phase (0, 0.2 0.4, 0.6, 0.8mg/ml) to get the working standard solutions for the preparation of the standard curve. Then saturated solutions of co-crystals **1-3** are prepared to be measured by HPLC, and the results of the solubility were obtained through the standard curve. For instance, the solubility of ambroxol is 12.9mg/ml at 40°C while the co-crystal **1** is 43.4mg/ml amount to 31.2mg/ml of ambroxol under the same conditions. The solubility of ambroxol and three co-crystals at different temperature were shown in **Figure 7**. In addition, we found co-crystal strategy could enhance the solubility greatly and an interesting phenomenon: the solubility of three co-crystals follow such order, co-crystal **1** < co-crystal **2** <

co-crystal **3**. It may be due to more O-H group in co-crystal **3** than co-crystals **1-2**.

## 5 Conclusions

In summary, we have presented the synthesis, crystal structure, Hirshfeld surface, thermal analysis (DSC and TGA) and Fluorescence spectroscopy of three novel co-crystals. By using these methods, especially surface and fingerprint plot analysis, we have an insight into not only detail analysis the intermolecular interactions of ambroxol molecules in the three co-crystals but also the kind of interactions contributing most to the stabilization of the three co-crystals. We found that the emission wavelength of three co-crystals follow this order: co-crystal **1** < co-crystal **2** < co-crystal **3**, which is consistent with H...H interactions of Hirshfeld surfaces analysis: co-crystal **1** (29.1%) < co-crystal **2** (35.7%) < co-crystal **3** (38.6%). Besides, the studies of the solubility also showed that more O-H group in guest molecules could enhance the solubility of host molecules and this co-crystal strategy provides a facile way to design and develop new co-crystals with good solubility, which is very important for bioavailability.

## Acknowledgements

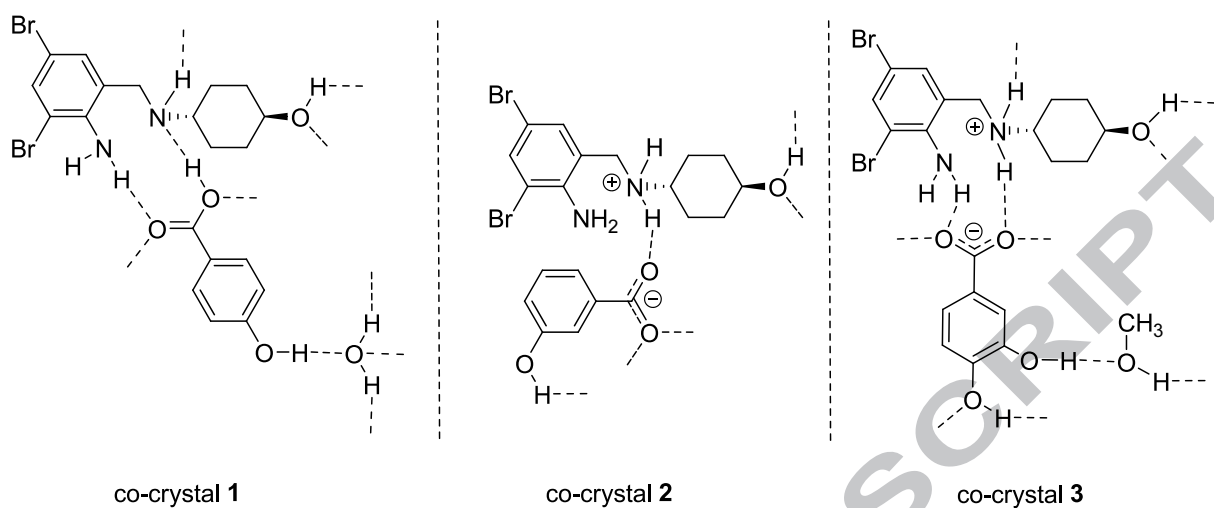
This work has been supported by the prospective joint research project of Jiangsu province (BY2012193) and the Fundamental Research Funds for the Central Universities (CXZZ12\_0119).

## References

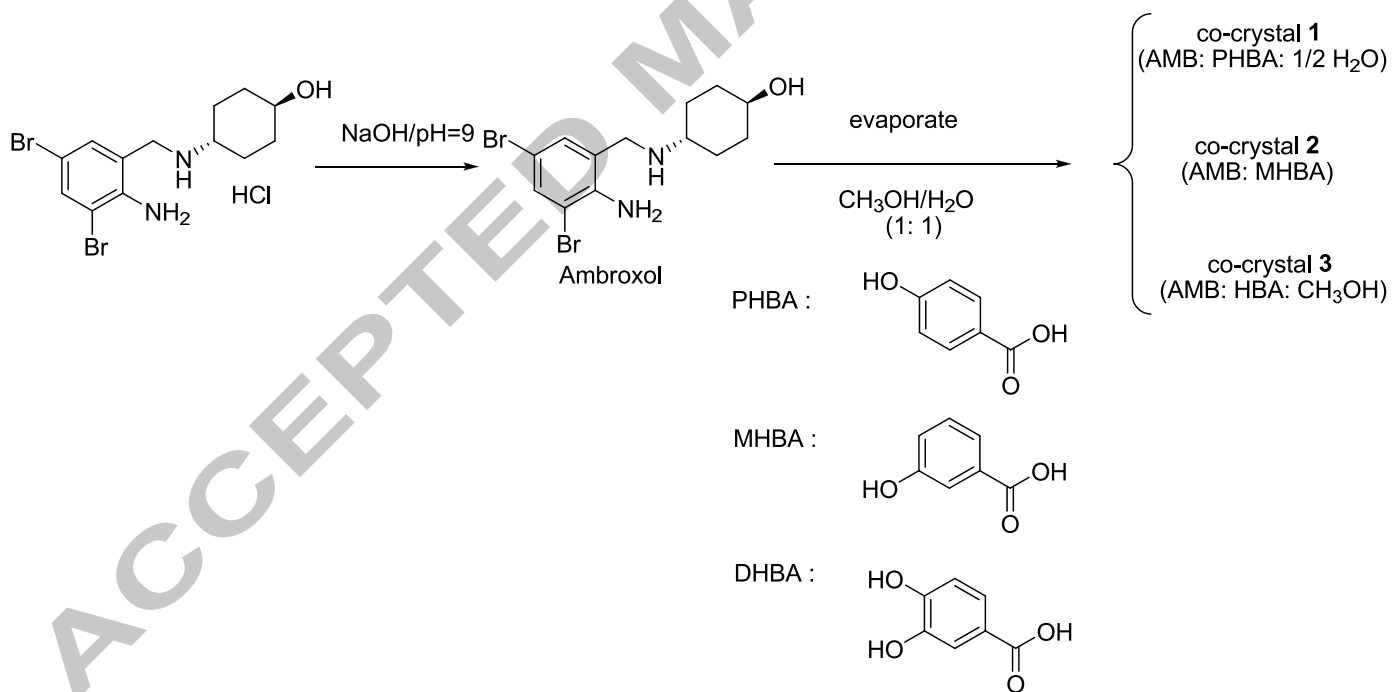
1. (a) J. Schmidt, W. Snipes, *Int. J. Radiat. Biol.* 13 (1967) 101; (b) M.C. Etter, *J. Phys. Chem.* 95 (1991) 4601.
2. N. Schultheiss, A. Newman, *Cryst. Growth Des.* 9 (2009) 2950.
3. J.Z. Schpector, E.R.T. Tiekink, *Z. Kristallogr.* 223 (2008) 233.
4. M. Khan, V. Enkelmann, G. Brunklaus, *J. Am. Chem. Soc.* 132 (2010) 5254.
5. J.M. Lehn, *Pure Appl. Chem.* 66 (1994) 1961–1966.
6. ö. Almarsson, M.J. Zaworotko, *Chem. Commun.* (2004) 1889–1895.
7. (a) A.V. Trask, W.D.S. Motherwell, W. Jones, *Int. J. Pharm.* 320 (1-2) (2006) 114; (b) N.J. Babu, A. Nangia, *Cryst. Growth Des.* 11 (2011) 2662; (c) A.N. Sokolov, T. Friscic, L.R. MacGillivray, *J. Am. Chem. Soc.* 128 (2006) 2806.
8. (a) Aakeroy, C. B.; Forbes, S.; Desper, J. *J. Am. Chem. Soc.* 2009, 131(47), 17048–17049. (b) Stanton, M. K.; Bak, A. *Cryst. Growth Des.* 2008, 8 (10), 3856–3862. (c) Nehm, S. J.; Rodriguez-Spong, B.; Rodriguez-Hornedo, N. *Cryst. Growth Des.* 2006, 6 (2), 592–600. (d) Cooke, M. W.; Stanton, M.; Shimanovich, R.; Bak, A. *Am. Pharm. Rev.*

- 2007, 10 (7), 54–59.
9. (a) Remenar, J. F.; Morissette, S. L.; Peterson, M. L.; Moulton, B.; MacPhee, J. M.; Guzmán, H. R.; Almarsson, O. J. *Am. Chem. Soc.* 2003, 125 (28), 8456–8457. (b) Schultheiss, N.; Lorimer, K.; Wolfe, S.; Desper, J. *CrystEngComm*. 2010, 12 (3), 742–749.
  10. A.K. Kruthiventi, I. Javed, S.R. Jaggavarapu, R. Nagalapalli, G.S. Viswanadha, S.K. Anand, US2012/0258170.
  11. J.H. Ter Horst, M.A. Deij, P.W. Cains, *Cryst. Growth Des.* 9 (2009) 1531.
  12. W. Jones, *MRS Bull.* 31 (2006) 875.
  13. W. Jones, in: W. Jones (Ed.), *Organic Molecular Solids: Properties and Applications*, CRC Press, New York, 1997, p. 177.
  14. A.D. Bond, W. Jones, in: W. Jones, C.N.R. Rao (Eds.), *Supramolecular Organisation and Materials Design*, Cambridge University Press, Cambridge, 2002, p. 391
  15. J.L. Atwood, J.E.D. Davies, D.D. MacNicol, F. Vogtle, *Comprehensive Supramolecular Chemistry*, vol. 9, Pergamon, Oxford, 1996.
  16. (a) Sanderson RJ et al. *Respir Phys.* (1976), 27 (3): 379–92. (b) Kido H et al. *Biol Chem.* (Nov 2004), 385 (11): 1029–34.
  17. (a) H. Suyama, N. Burioka, T. Sako, Y. Kawasaki, Y. Hitsuda, K. Shigeshiro, Y. Matsumoto, *Yonago Acta Medica*, 42 (1999) 175. (b) Y. H. Luo, G. G. Wu, B.W. Sun, *Journal of Chemical & Engineering Data*, 58 (2013) 588. (c) F. Segura-Lozano, G. Tenorio, *Rev. Med. Hosp. Gen. Mex.*, 58 (1995) 118.
  18. V.A. Blatov, A.P. Shevchenko, V.N. Serezhkin, *Zh.Strukt. Khim* 34 (1993) 83–85..
  19. T. Gelbrich, M.B. Hursthouse, *CrystEngComm* 7 (2005) 324–336.
  20. S.K. Wolff, D.J. Grimwood, J.J. McKinnon, D. Jayatilaka, M.A. Spackman, *CrystalExplorer1.5*, University of Western Australia, Perth, Australia..
  21. F.P.A. Fabbiani, L.T. Byrne, J.J. McKinnon, M.A. Spackman, *CrystEngComm* 9 (2007) 648–652..
  22. A. Parkin, G. Barr, W. Dong, C.J. Gilmore, D. Jayatilaka, J.J. McKinnon, M.A. Spackman, C.C. Wilsona, *CrystEngComm* 9 (2007) 648–652.
  23. Y.H. Luo, J. Xu, B.W. Sun, *Journal of Chemical Research* (2012) 697–700..
  24. Y.H. Luo, C.G. Zhang, B. Xu, B.W. Sun, *CrystEngComm* 14 (20) (2012) 6860–6868.
  25. G.M. Sheldrick, *SHELXL-97: Program for the Refinement of Crystal Structures*, University of Gottingen, Germany, 1997.
  26. Y.H. Luo, M.L. Pan, *Acta Crystallography E* 68 (2012) o206.
  27. Y.H. Luo, J. Xu, M.L. Pan, J.F. Li, *Acta Crystallography E* 67 (2011) o2099.
  28. CCDC, Cambridge, U.K., 2003–2004.
  29. (a) S. Tothadi, S. Joseph, G.R. Desiraju *Cryst. Growth Des.* 13 (2013) 3242–3254; (b) A. D. Santis, A. Forni, R. Liantonio, P. Metrangolo, T. Pilati, G. Resnati. *Chem. Eur. J.* 9 (2003) 3974–3983.

## Figures and schemes



**Scheme.1** Hydrogen bonding synthons identified in the crystal structure of co-crystals 1-3



**Scheme.2** The preparations of co-crystals 1-3

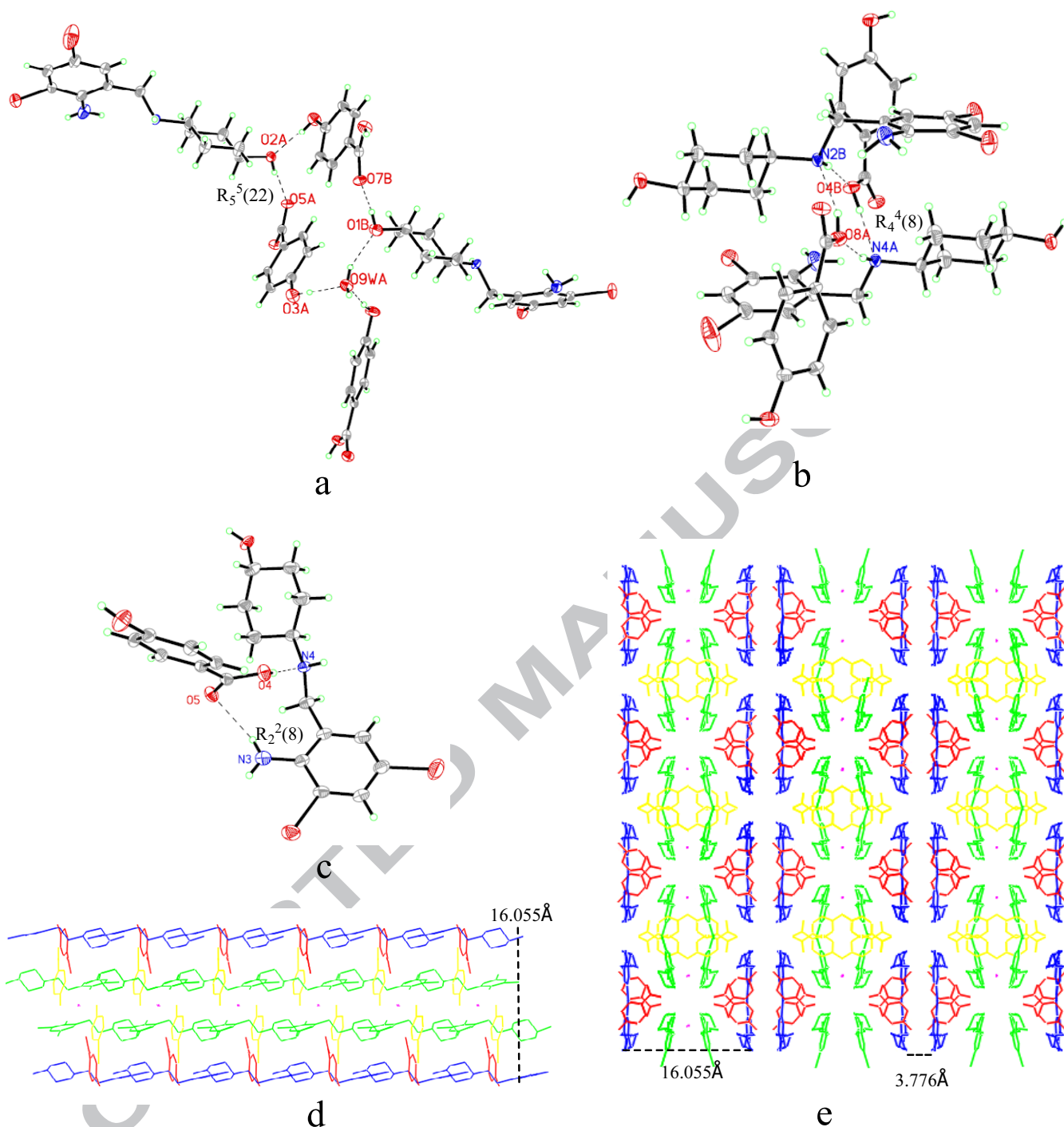


**Figure.1** Molecular structure of co-crystal **1**, hydrogen bonds formed by  $\text{H}_2\text{O}$  molecule are in dashed lines and supramolecular synthons around the  $R_5^5(22)$  pentameric unit (a); hydrogen bonds formed by two AMB molecules and two PHBA molecules and supramolecular synthons around the  $R_4^4(8)$  tetrameric unit (b); dimeric unit with one AMB molecule and one PHBA by  $R_2^2(8)$  supramolecular heterosynthon through  $\text{N-H}\cdots\text{O}$  (c); a typical layer viewed from  $b$ -axis (d); crystal packing stabilized by an obvious  $\pi \cdots \pi$  intermolecular interactions were observed with plane separation of  $3.776 \text{ \AA}$  and the 2D sheet extended in the crystallographic  $ab$  plane (e).

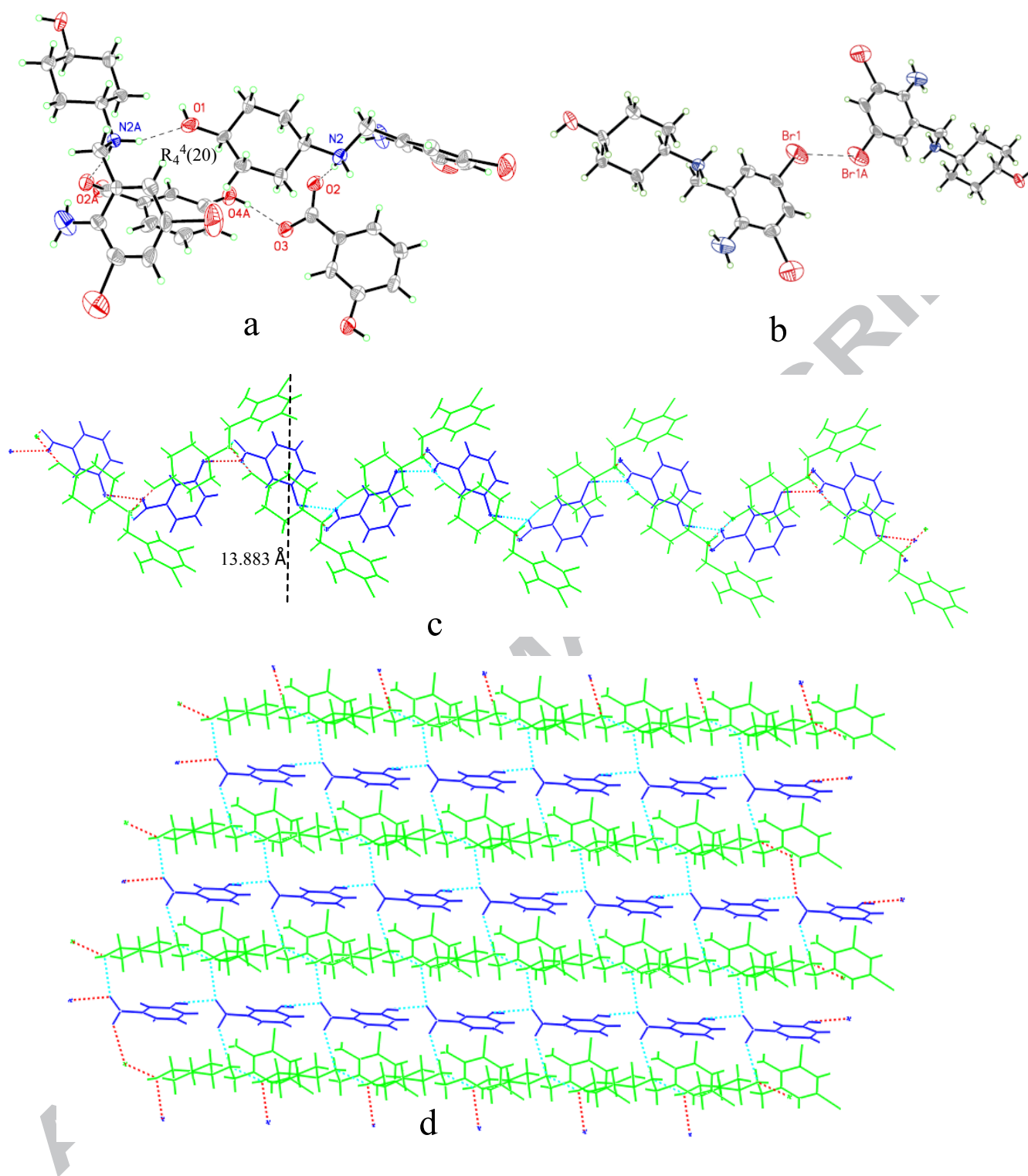


**Figure.2** Molecular structure of co-crystal 2, tetrameric unit by  $R_4^4(20)$  supramolecular heterosynthesis and hydrogen bonds are in dashed lines (a); the  $\text{Br} \cdots \text{Br}$  interaction with the distance of 3.585 Å (b); zigzag motif of a typical layer viewed from a-axis (c); the 2D network extended in the crystallographic ac plane (d).

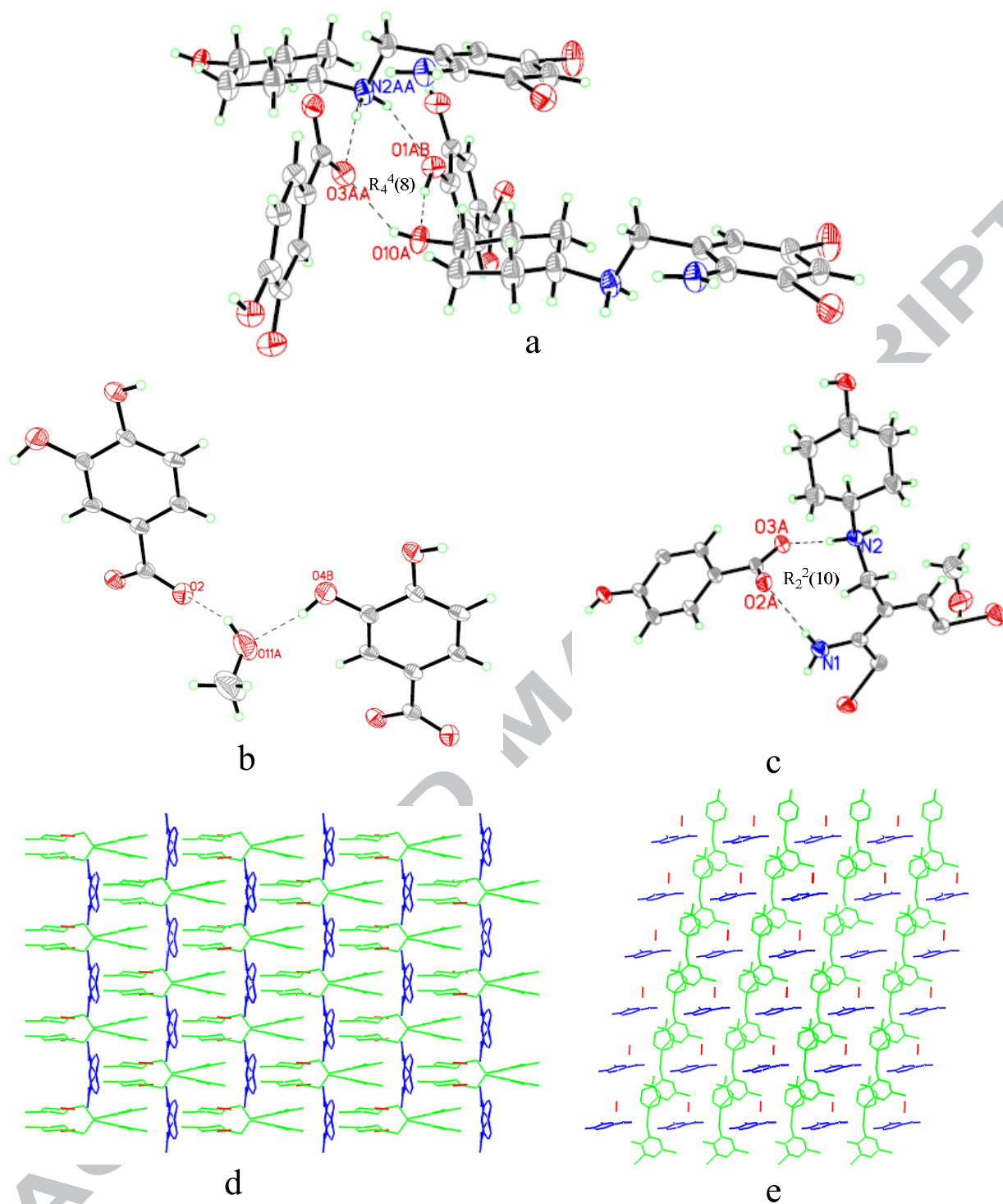


**Figure.3** Molecular structure of co-crystal **3**, hydrogen bonds formed by two AMB molecules and two entire DHBA molecules are in dashed lines and supramolecular synthons around the  $R_4^4(8)$  tetrameric unit (a); hydrogen bonds formed by one AMB molecule and one DHBA molecule and supramolecular synthons around the  $R_2^2(10)$  dimeric unit (b); hydrogen bonds formed by one  $\text{CH}_3\text{OH}$  molecule and two DHBA molecules through the  $\text{O}-\text{H}\cdots\text{O}$  hydrogen bonds (c); the 2D network extended in the crystallographic  $ab$  plane (d); 2D network extended in the crystallographic  $ac$  plane (e).

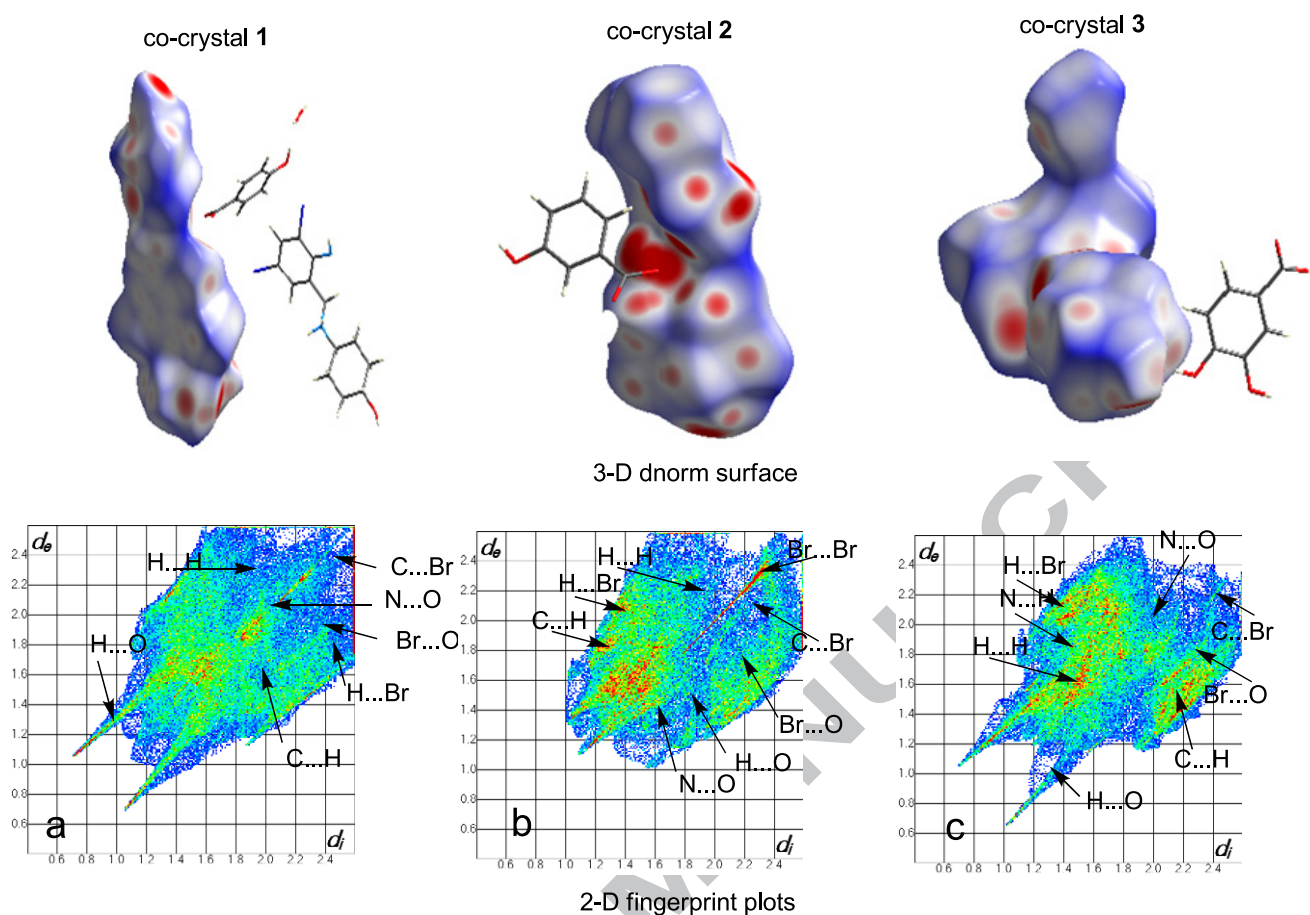


**Figure.4** 3-D  $d_{norm}$  surfaces and 2-D fingerprint plots of AMB in co-crystals 1-3.

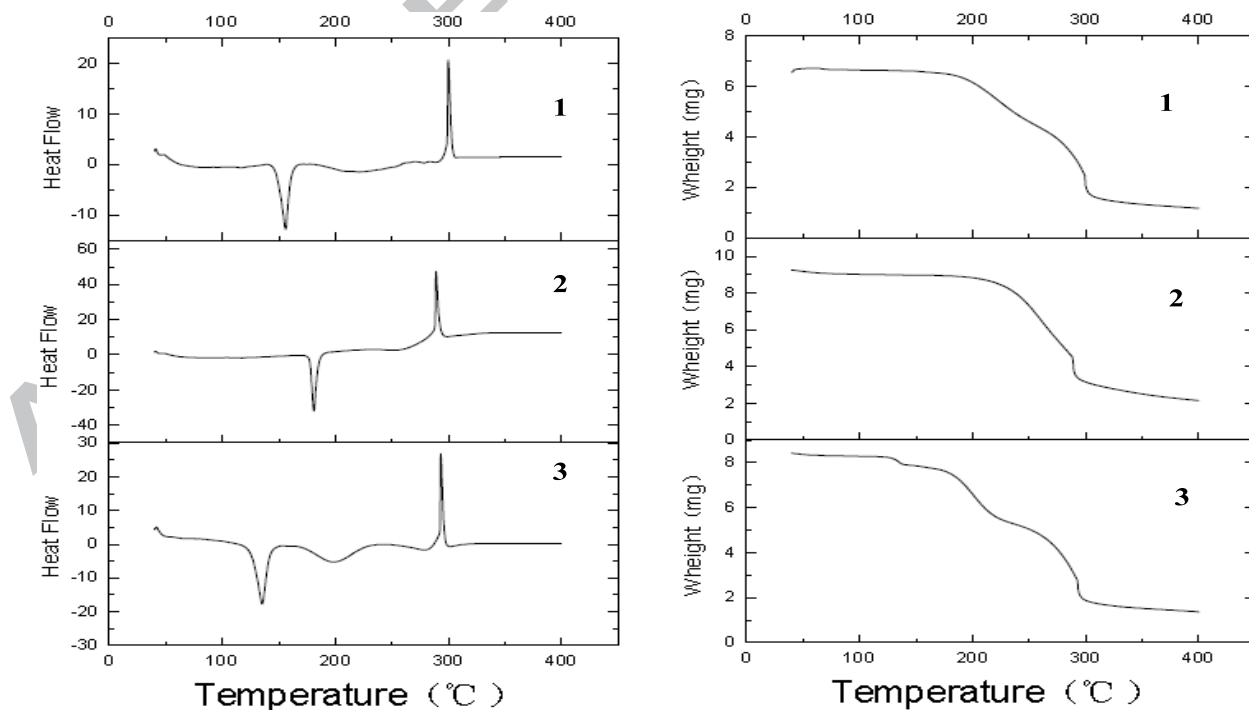


**Figure.5** The DSC (left) and TGA (right) profiles of co-crystals 1-3.

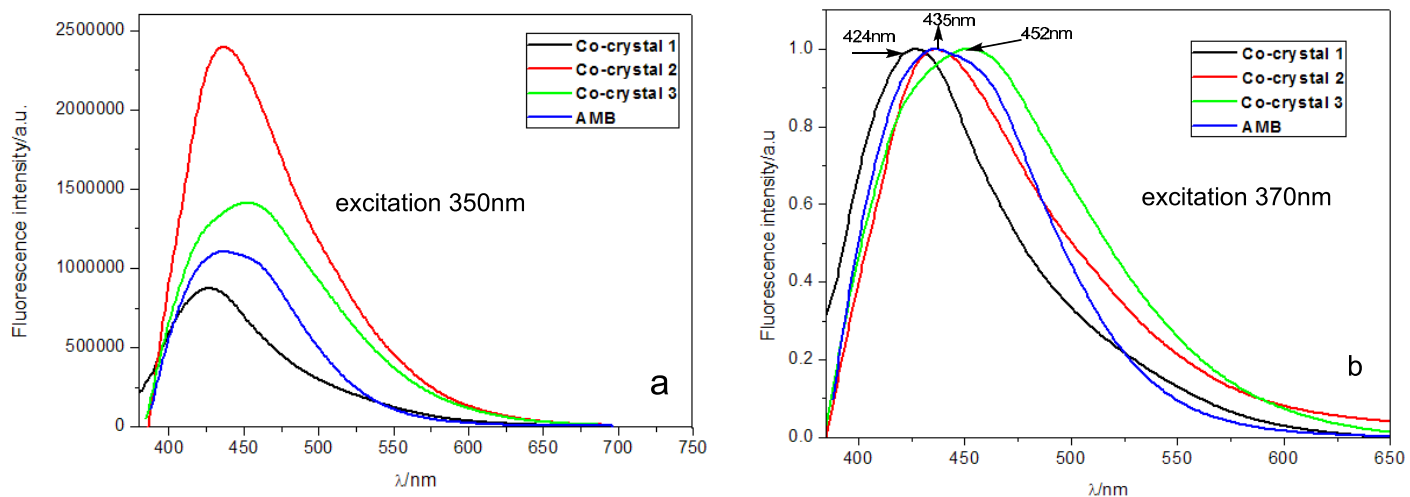


**Figure.6** Fluorescence spectra of three co-crystals (a) and the figure of normalization (b)

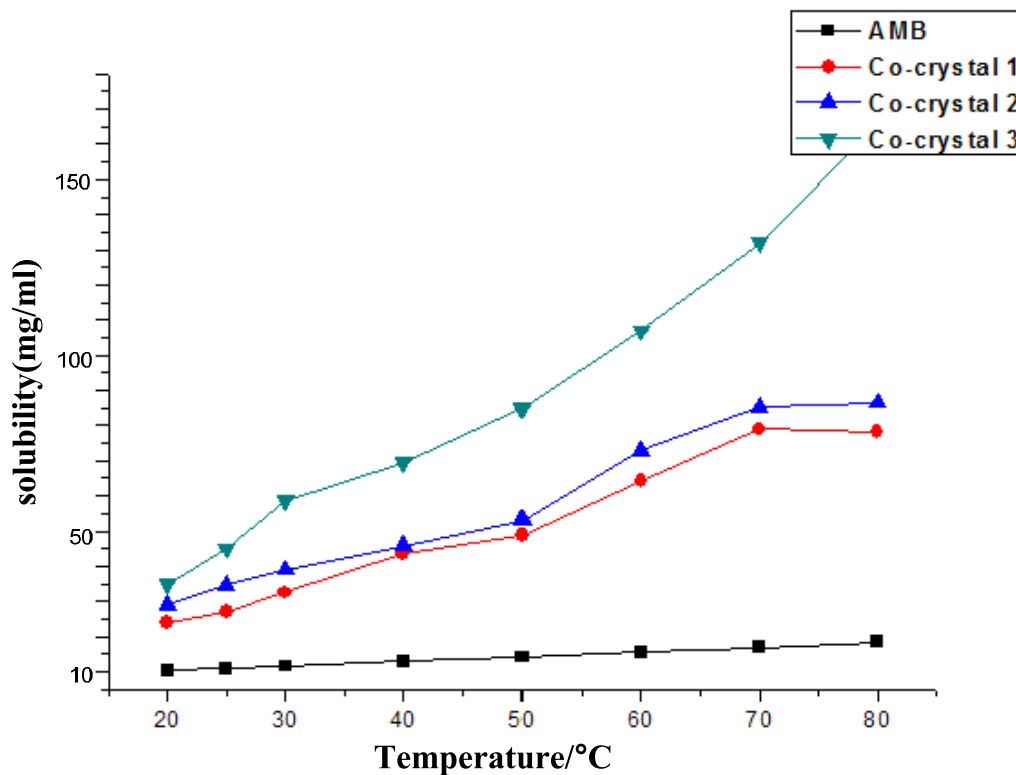


**Figure.7** Solubility of ambroxol and the three co-crystals at different temperature

## Tables

**Table.1** Crystal Datas and Structure Refinement for co-crystals **1-3**

	co-crystal <b>1</b>	co-crystal <b>2</b>	co-crystal <b>3</b>
Empirical formula	C <sub>80</sub> H <sub>98</sub> Br <sub>8</sub> N <sub>8</sub> O <sub>17</sub>	C <sub>20</sub> H <sub>24</sub> Br <sub>2</sub> N <sub>2</sub> O <sub>4</sub>	C <sub>41</sub> H <sub>58</sub> Br <sub>4</sub> N <sub>4</sub> O <sub>12</sub>
Formula weight	2082.86	516.21	1116.50
wavelength(A)	0.71073	0.71073	0.71073
crystal system	monoclinic	monoclinic	monoclinic
space group	P 2/c	P 21/n	C c
a, Å	19.305(4)	8.6641(17)	15.246(3)
b, Å	14.971(3)	19.675(4)	8.6014(17)
c, Å	15.933(3)	12.862(3)	18.704(4)
$\alpha$ (°)	90.00	90.00	90.00
$\beta$ (°)	111.16(3)	102.83	102.87(3)
$\gamma$ (°)	90.00	90.00	90.00
V, Å <sup>3</sup>	4294.4(17)	2137.7(7)	2391.2(8)
Z	2	4	2
T/K	293(2)	293(2)	293(2)
Density (calculated), g/cm <sup>3</sup>	1.611	1.604	1.554
Absorption coefficient, mm <sup>-1</sup>	3.804	3.820	3.427
<i>h, k, l</i> (min, max)	(-23,23), (-18,18),(-19,19)	(-11,11),(-25,25),(-16, 16)	(-18,18),(-10,10),(- 22,22)
Parameters	536	255	285
F(000)	2100	1040	1136
Goodness-of-fit on F2	1.040	1.007	1.036
Final R indices [I>2 $\sigma$ (I)]	R1=0.0628 $\omega$ R2=0.1416	R1=0.0830 $\omega$ R2=0.2424	R1=0.0740 $\omega$ R2=0.2072

**Table.2** Geometrical parameters for the hydrogen bonds, C-H... $\pi$ ,  $\pi$ ... $\pi$  and Br...X (-H, -C, or -Br) interactions in co-crystals **1-3**

	D-H...A	D-H (Å)	H...A (Å)	D...A (Å)	<D-H...A(deg )	symmetry code	
Co-crystal <b>1</b>	O9W-H9D...O1	0.69	2.14	2.66	132	x,y,1+z	
	O1-H1D...O7	0.82	1.88	2.639	154	x,y,-1+z	
	O2-H2...O5	0.82	1.92	2.734	171	x,1-y,1/2+z	
	N2-H2A...O4	0.74	2.03	2.767	173		
	N4-H4A...O8	0.78	2.01	2.77	168	x,-y,-1/2+z	
	O3-H3...O9W	0.82	1.88	2.698	174	1-x,1-y,1-z	
	O6-H6...O2	0.82	1.89	2.711	174		
	N1-H10W...Br1	0.88	2.58	3.077	117		
	N3-H3B...O5	0.86	2.4	2.942	121		
	O4-H4...N4	0.82	1.95	2.755	165		
	O8-H8W...N2	0.82	2	2.778	158	x,-y,1/2+z	
	N1-H10Y...O7	0.90	2.00	2.873	164	x,-y,-1/2+z	
	C21-H21...O6	0.98	2.44	3.301	147	-x,y,1/2-z	
Co-crystal <b>2</b>	C26-H26A...O8	0.97	2.55	3.236	128	x,-y,-1/2+z	
	N2-H2A...O1	0.9	1.98	2.819	154	1/2+x,1/2-y,1/2+z	
	N2-H2B...O2	0.9	1.85	2.733	168	-1/2+x,1/2-y,1/2+z	
						z	
	O4-H4...O3	0.82	1.81	2.621	168	1/2+x,1/2-y,1/2+z	
	N1-H1Y...O2	0.86	2.5	3.215	142	-1/2+x,1/2-y,1/2+z	
						z	
	Co-crystal <b>3</b>	C8-H8...O4	0.98	2.51	3.470	165	
		O1-H1...O10	0.82	1.9	2.686	161	1/2+x,-1/2+y,z
		O4-H4...O11	0.82	1.83	2.628	165	-1/2+x,-1/2+y,z
O10-H10...O3		0.82	1.98	2.677	142	-1/2+x,1/2-y,-1/2+z	
						z	
O11-H11A...O2		0.82	2.14	2.63	119	1/2+x,-1/2+y,z	
N1-H1B...O2		0.85	2.12	2.914	156	x,1-y,-1/2+z	
N2-H2B...O2		0.9	2.52	3.178	130	x,1-y,-1/2+z	
N2-H2B...O3		0.9	1.87	2.761	172	x,1-y,-1/2+z	
N2-H2A...O1		0.9	2.09	2.861	143	x,1+y,z	
Co-crystal <b>1</b>	N1-H1C...Br2	0.86	2.63	3.06	112		
	C21-H21A...O4	0.97	2.47	3.409	163	x,1+y,z	
	C-H... $\pi$		H...Cg	X...Cg	X-H...Cg	symetry code	
	C1-H1...Cg(5) <sup>a</sup>		2.62	3.478	154	x,1-y,1/2+z	
C13-H13b... Cg(3) <sup>b</sup>		2.94	3.576	124	x,y,z		

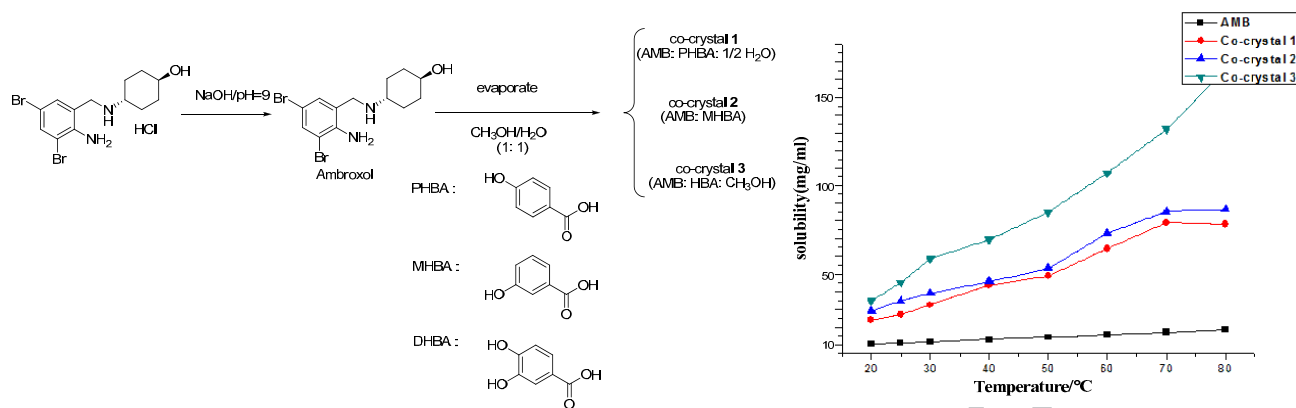
	C14-H14...Cg(6) <sub>c</sub>	2.83	3.761	176	x,y,-1+z
	C26-H26B...Cg(1) <sup>d</sup>	2.75	3.551	140	x,y,z
Co-crystal 3	C7-H7... Cg(3) <sup>e</sup>	2.73	3.588	154	1/2+x,1/2+y,z
	$\pi \cdots \pi$		Cg...Cg		symetry code
Co-crystal 1	Cg(3) ...Cg(3) <sup>b</sup>		3.776		-x,y,-1/2-z
	At(I) ...At(J)		D(I...J)(Å )	Sumrad Del	symetry code
Co-crystal 1	Br(1) ...H(36)		3.01	3.05 -0.04	
	Br(3) ...C(29)		3.531	3.55-0.02	x,1-y,1/2+z
Co-crystal 2	Br(1) ...Br(1)		3.585	3.70-0.11	2-x,-y,2-z

a: 6-Membered Ring C(27)→C(28)→C(29)→C(30)→C(31)→C(32); b: 6-Membered Ring C(14)→C(15)→C(16)→C(17)→C(18)→C(19); c: 6-Membered Ring C(34)→C(35)→C(36)→C(37)→C(38)→C(39); d: 6-Membered Ring C(1)→C(2)→C(3)→C(4)→C(5)→C(6); e: 6-Membered Ring C(1)→C(2)→C(15)→C(5)→C(4)→C(3).

**Table.3** Summary of the various contact contributions to the AMB Hirshfeld surface area in co-crystals 1-3

	co-crystal 1 (%)	co-crystal 2 (%)	co-crystal 3 (%)
H-H	29.1	35.7	38.6
H-O	24.5	18.5	20.8
H-Br	19.6	21.8	19.8
C-H	13.5	17.8	16
N-H	5.2	2.0	1.2
N-O	1.7	0.9	0.1
C-Br	2.2	1.5	0.9
Br-Br	1.1	1.0	0
Br-O	0.5	0.6	1.6

## Graphical abstract



**Highlight**

- 1 . Three novel pharmaceutical co-crystals have been structurally characterized
2. The O–H···O, O–H···N, N–H···O and N–H···Br hydrogen bonds between host and guest molecules have been analyzed.
3. The intermolecular interactions have also been analyzed by Hirshfeld surfaces analysis.

ACCEPTED MANUSCRIPT